Double resonance 1-D photonic crystal cavities for single-molecule mid-infrared photothermal spectroscopy: theory and design

Hongtao Lin, Zou Yi, and Juejun Hu*

Department of Materials Science & Engineering, University of Delaware, Newark, Delaware 19716, USA
**Corresponding author: hujuejun@udel.edu*

Received December 1, 2011; revised January 10, 2012; accepted February 15, 2012;
posted February 15, 2012 (Doc. ID 158439); published April 6, 2012

We propose and theoretically examine a novel mid-infrared (mid-IR) photothermal spectroscopic sensing technique capable of detecting a single small molecule. Our conceptual design attains such high sensitivity by leveraging dramatically amplified photothermal effects in an optical nanocavity doubly resonant at both mid-IR pump and near-IR probe wavelengths. Unlike conventional mid-IR spectroscopy, the technique eliminates the need for cryogenically cooled mid-IR photodetectors, as optical detection is performed solely at the near-IR probe wavelength. A device design based on nested one-dimensional nanobeam photonic crystal cavities is numerically analyzed to demonstrate the technique's potential for single small gas molecule detection.

OCIS codes: 300.6430, 230.5298, 140.3945, 130.6010.

"Sensor-on-a-chip" devices are attracting considerable interest recently owing to their dramatically reduced footprint, power consumption and cost per test compared to conventional bench top instruments. On-chip optical sensors using infrared (IR) absorption spectroscopy have been demonstrated with a limit of detection (LOD) of about 0.001 cm^{-1} in terms of analyte absorption coefficient, corresponding to parts-per-million (ppm) sensitivity for gas sensing [1–4]. This LOD figure is far inferior compared to free-space IR spectroscopy, which is capable of trace gas detection down to the parts-per-billion (ppb) level [5,6]. High propagation loss of planar waveguide devices (~dB/cm) and the short optical path length accessible on a chip limits the photon-molecule interaction strength, which accounts for this vast sensitivity gap. Additionally, as the absorption fingerprints of most molecules are located in the mid-IR spectral region, cryogenically cooled mid-IR photodetectors (e.g. HgCdTe detectors) are required for optical detection [2], which poses a significant challenge to planar integration and cost reduction.

Here we present a novel IR photothermal spectroscopy technique using suspended photonic crystal (PhC) nanobeam cavities (Fig. 1)to solve both the sensitivity and mid-IR detection challenges facing current methods. The following is a description of this technique. A mid-IR pump beam whose wavelength is tuned to match a characteristic absorption line of target molecules is launched into the cavity to induce optical absorption and photothermal effect. Heat generated in the absorption process leads to a temperature rise of the suspended cavity, which induces thermo-optic resonance spectral shift at the probe wavelength. The resonance shift is subsequently detected using a low-power near-IR probe beam to quantify the target species concentration. Two mechanisms underlie the ultrahigh sensitivity of the new technique: (1) the photothermal interaction strength is drastically amplified due to both optical resonance enhancement and thermal confinement, simultaneously achieved through material design and device engineering; (2) since elastic scattering does not generate photothermal signal (heat), background noise due to optical scattering loss in planar high-index-contrast waveguide devices is minimal. Noise from environmental temperature fluctuations can be mitigated by adding a reference cavity for differential measurement. Furthermore, since mid-IR absorption is translated into photothermal resonance shift at the near-IR probe wavelength, the technique can operate using low-cost, high performance photodiodes at telecommunication bands rather than resorting to mid-IR detectors made of exotic semiconductor alloys.

Our previous work [7] derived a simplified theory of cavity-enhanced photothermal spectroscopic sensing using a lumped circuit model and in the special case of degenerate pump/probe wavelengths. In this letter, we extend the analysis to generic photothermal sensing configurations. Denote the loaded quality (Q) factor at the pump wavelength as Q_{pu} and assuming critical coupling.

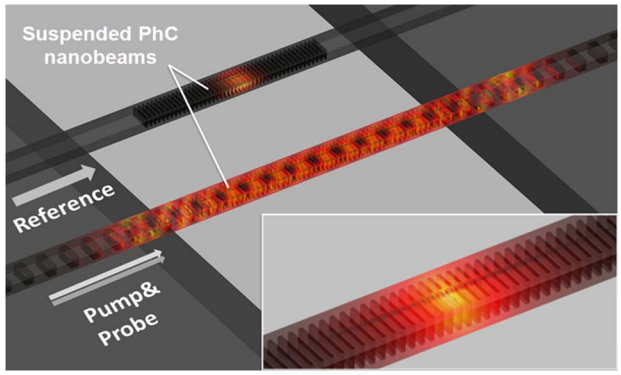

Fig. 1. (Color online) Tilted view of a suspended double resonance PhC nanobeam sensor cavity and a reference cavity; optical absorption by target analyte molecules at the pump wavelength leads to photothermal heat generation and temperature rise, which is detected through the thermo-optic resonance shift at the probe wavelength. The color represents optical field intensity distribution in the cavities.

The photothermal heat generation rate due to pump absorption by a single molecule in the cavity is

$$P_c(\mathbf{r}_0) = \frac{1}{2\pi}\lambda_{\mathrm{Pu}}\sigma P_{\mathrm{pu}} Q_{\mathrm{pu}} \varepsilon_c(\mathbf{r}_0)|E_{N,\mathrm{pu}}(\mathbf{r}_0)|^2, \quad (1)$$

where λ_{pu} is the pump wavelength, σ is the optical absorption cross-section of the molecule, P_{pu} is the optical pump power coupled into the cavity, ε_c is the spatially dependent cavity dielectric constant distribution, $E_{N,\mathrm{pu}}$ is the dimensionless cavity eigenmode at λ_{pu}, normalized so $\int \varepsilon_c|E_{N,\mathrm{pu}}|^2 \mathrm{d}V = 1$, where the integration is carried out throughout the entire cavity, and $\mathbf{r}_0$ denotes the position vector of the point heat source where the molecule resides. The heat source term defined by Eq. (1) can be then be used in conjunction with the thermal transport equation to calculate the temperature profile:

$$-\nabla \cdot [\kappa(\mathbf{r})\nabla T(\mathbf{r})] = P_c(\mathbf{r}_0) \cdot \delta^3(\mathbf{r} - \mathbf{r}_0), \quad (2)$$

where κ is the thermal conductivity, and T is the cavity temperature. Both parameters are spatially dependent. Apparently, using cavity materials with low thermal conductivity contributes to enhanced photothermal effect.

The probe resonance wavelength shift is thus given by the cavity perturbation theory as:

$$\Delta\lambda_{\mathrm{pr}} = \lambda_{\mathrm{pr}} \cdot \frac{\int \frac{dn}{dT} \cdot n(\mathbf{r}) \cdot \Delta T(\mathbf{r}) \cdot \varepsilon_0 |E_{\mathrm{pr}}(\mathbf{r})|^2 \mathrm{d}V}{\int \varepsilon_c |E_{\mathrm{pr}}(\mathbf{r})|^2 \mathrm{d}V}, \quad (3)$$

where λ_{pr} is the probe resonance wavelength and the integration is performed over the entire cavity volume. The temperature rise $\Delta T(\mathbf{r}) = T(\mathbf{r}) - T_0$ is proportional to the cavity Q actor at pump wavelength up to the onset of absorption saturation, beyond which further increasing Q_{pu} has a diminishing return on sensitivity improvement [8]. Since our previous analysis has established that wavelength resolution of the probe resonance shift is primarily limited by temperature fluctuations of the ambient environment rather than by the finite resonant peak spectral width [9], a moderate probe Q-factor of $\sim 10^6$ suffices to achieve background-thermal-noise-limited operation. Finally, it should be noted that even though the cavity mode volume does not enter Eq. (3) explicitly, a small cavity mode volume enhances the photothermal effect since the thermal conductance (leakage) is proportional to the cavity linear dimensions.

Based on the optical and thermal design considerations, a cavity material figure of merit (FOM) is defined:

$$\mathrm{FOM} = n \cdot \kappa^{-1} \cdot \frac{dn}{dT}, \quad (4)$$

where n is the refractive index (optical confinement), κ denotes the thermal conductivity (thermal isolation), and dn/dT is the thermal-optic coefficient (the ability to convert temperature change to resonance shift). Table 1 lists the FOMs of a commercially available chalcogenide glass (ChG) IG3 [10], silicon, and silica. Clearly, the material FOM of IG3 glass is over 100 times higher than those of silica and silicon! Other properties of ChGs, such as low optical loss [11,12], good chemical durability, as well as capacity for monolithic integration on different substrates, further justify the selection.

Table 1. Material Properties Relevant to Photothermal Sensing

Material	n	κ (W/mK)	dn/dT (K^{-1})	FOM m/W
IG3 Glass	2.81	0.22	1.3×10^{-4}	1.6×10^{-3}
Silicon	3.45	149	2.3×10^{-4}	5.2×10^{-6}
SiO_2	1.45	1.38	1.0×10^{-5}	1.0×10^{-5}

Figure 2 shows top views of the proposed suspended ChG glass PhC nanobeam design consisting of two nested cavities, supporting resonances at 1.55($Q_{\mathrm{pr}} = 1.37 \times 10^6$) and 5.27 μm wavelengths ($Q_{\mathrm{pu}} = 40,200$), respectively. Both pump and probe cavities adopt a size-modulated design to achieve high-Q operation [13]. The 5.27 μm pump wavelength is chosen to match the absorption line of nitric oxide (NO) molecules and serves only as an illustrative example here: the pump resonance wavelength can be easily tuned by adjusting the photonic crystal period. The nanobeam device uniquely combines sub-diffraction-limit optical confinement, superior thermal isolation, as well as high optical Q-factors at both pump and probe wavelengths. All are desirable features for nanocavity photothermal detection.

The cavity is optimized based on the following criteria:

(1) The cavity Q-factors at pump and probe wavelengths are fine-tuned by adjusting the number of Bragg mirror segments. We target a lower pump wavelength Q-factor ($Q_{\mathrm{pu}} = 40,200$) on purpose for two reasons: (a) The relatively broad pump resonance enables spectral scan across the sharp absorption lines of gas molecules resolving the fine spectral features. For example, the doublet absorption line of NO at 1897 cm^{-1} has a FWHM spectral width of 0.002 cm^{-1}, much narrower than the PhC pump resonance peak [14]. (b) The absorption saturation effect (similar to photobleaching, which diminishes optical absorption) poses an upper limit of $\sim 50,000$ to Q_{pu} [8]. The high Q-factor at the probe wavelength ($Q_{\mathrm{pr}} = 1.37 \times 10^6$) offers subpicometer resolution necessary for ultrasensitive spectral shift detection. In our optimized design, the probe wavelength cavity is sandwiched between 15 mirror segments and 7 taper segments. The pump wavelength cavity consists of 3 mirror segments and 14 taper segments on each side of the cavity. Tapers are inserted between the two sets of mirror segments to eliminate scattering loss.

(2) Spatial overlap between the probe resonance mode and the cavity temperature rise profile is maximized, as is suggested by Eq. (3). In our design, the probe resonance mode coincides with the peak location of the pump resonance mode where heat generation is also maximum.

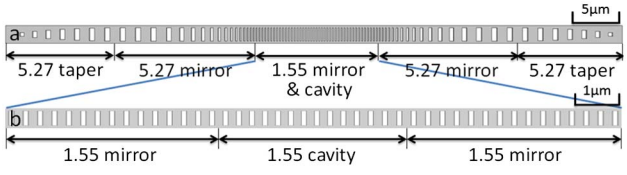

Fig. 2. (Color online) (a) Top view of the double resonance ChGPhC nanobeam cavity design; (b) enlarged top-view of the 1.55 μm probe wavelength cavity.

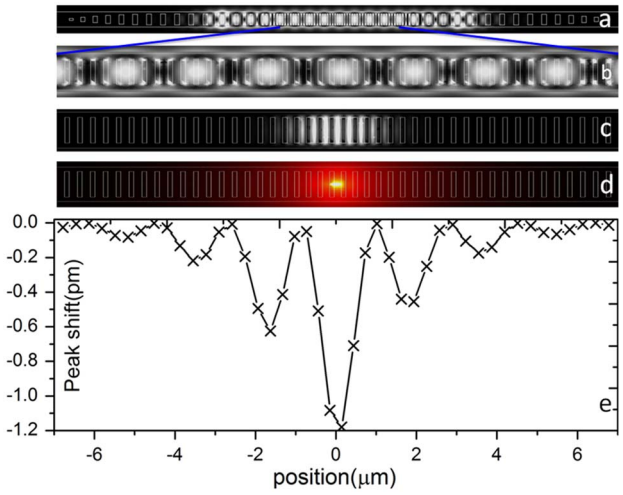

Fig. 3. (Color online) Optical field intensity distribution of resonance mode at (a) (b) 5.27 μm wavelengths (b) shows a zoom-in view near the cavity center; (c) 1.55 μm wavelengths; (d) temperature distribution due to photothermal heat generation from a single moleculelocated at the cavity center; (e) single-molecule induced peak shift as a function of molecule position along the nanobeam. The same horizontal scale is used for (b)—(e).

(3) Insertion loss due to waveguide-cavity coupling is mitigated by using a Bloch mode engineering approach [15] to design the taper structure. The pump wavelength cavity is strongly coupled to the input waveguide by satisfying the condition that the coupling coefficient (mirror loss) is much larger than radiative loss inside the cavity, which guarantees efficient pump power delivery into the cavity. The insertion loss is determined by finite-difference time-domain (FDTD) simulations to be <0.5 dB, sufficiently small for our target application.

(4) To achieve high Q_{pr}, out-of-plane radiative loss from the cavities is minimized by carefully designed taper structure to linearly increase the mirror strengths of the Bragg reflector segments. Quan and Loncar have illustrated such a structure yields Gaussian-like cavity mode profiles with minimal radiative loss [16].

Spectroscopic sensing performance of the optimized device is evaluated using numerical simulations. The optical field intensity distributions of resonance modes are calculated using the FDTD method, as are shown in Figs. 3(a)–3(c). Temperature distribution in the cavity is subsequently determined by solving Eq. (1) using the built-in heat transfer model of COMSOL multiphysics package. Figure 3(d) shows the cavity temperature profile resulting from photothermal heat generation by a single molecule adsorbed onto the nanobeam surface. In this case, the molecule is placed at a location where the electromagnetic field is most intense at the pump wavelength. Citing an average absorption cross section of 3.0×10^{-18} cm^2 [14,17] for a single nitric oxide molecule at 5.27 μm wavelength and assuming a moderate pump power of 50 mW (power coupled into the cavity), which is readily attainable by current quantum cascade lasers, Eq. (3) yields a maximum photothermal resonance shift of 1.2 pm at the probe wavelength. Thermal stress and stress-optical coupling is also numerically calculated and is found to be only <1% of the direct thermo-optic effect. Such a resonance shift is sufficiently large to be detected by a traditional wavelength-sweeping technique. For example, S. Shopova *et al.* have recently demonstrated spectral resolution down to the 0.1 pm range using resonator refractometry [18]. It should be noted the photothermal wavelength shift is dependent on the molecule location: as is shown in Fig. 3(e), the peak shift maximizes when the molecule aligns with the field maxima. This observation is unique to single or few-molecule-level sensors where the discrete nature of molecules becomes non-negligible.

Given that at least one molecule must be present per cavity mode volume (2.2×10^{-11} cm^3) for detection to occur, a LOD in terms of gas concentration is calculated to be 1.7 ppb. This figure represents four orders of magnitude improvement compared to the LOD of current on-chip IR sensors [3,4].

In conclusion, we have theoretically analyzed a PhC nanobeam photothermal sensor design with LOD down to a single small molecule. The superior thermal and optical properties of ChG glasses, the double resonance cavity design, as well as our unique approach of combining dual optical-thermal confinement in the same nanobeam device account for the high sensitivity. The novel double resonance PhC cavity structure may also find applications in nonlinear frequency generation and quantum information processing.

The authors gratefully acknowledge start-up support provided by the University of Delaware.

References and Note

1. A. Ganjoo, H. Jain, C. Yu, R. Song, J. V. Ryan, J. Irudayaraj, Y. J. Ding, and C. G. Pantano, Non-Cryst J. Solids **352**, 584 (2006).
2. C. Charlton, A. Katzir, and B. Mizaikoff, Anal. Chem. **77**, 4398 (2005).
3. A. Nitkowski, L. Chen, and M. Lipson, Opt. Express **16**, 11930 (2008).
4. J. Hu, N. Carlie, L. Petit, A. Agarwal, K. Richardson, and L. C. Kimerling, J. Lightwave Technol. **27**, 5240 (2009).
5. G. Gibson, S. Monk, and M. Padgett, Mod J. Opt. **49**, 769 (2002).
6. A. Kosterev, Y. Bakhirkin, R. Curl, and F. Tittel, Opt. Lett. **27**, 1902 (2002).
7. J. Hu, Opt. Express **18**, 22174 (2010).
8. S. E. Bialkowski, Appl. Opt. **32**, 3177 (1993).
9. J. Hu, X. C. Sun, A. Agarwal, and L. C. Kimerling, J. Opt. Soc. Am. B **26**, 1032 (2009).
10. SCHOTT North America, "Infrared Chalcogenide Glass IG3."
11. S. Madden, D. Choi, D. Bulla, A. Rode, B. Luther-Davies, V. Ta'eed, M. Pelusi, and B. J. Eggleton, Opt. Express **15**, 14414 (2007).
12. J. Hu, N. Feng, N. Carlie, L. Petit, A. Agarwal, K. Richardson, and L. C. Kimerling, Opt. Express **18**, 1469 (2010).
13. J. Chan, M. Eichenfield, R. Camacho, and O. Painter, Opt. Express **17**, 3802 (2009).
14. D. Nelson, J. Shorter, J. McManus, and M. Zahniser, Appl. Phys. B **75**, 343 (2002).
15. M. Palamaru and P. Lalanne, Appl. Phys. Lett. **78**, 1466 (2001).
16. Q. Quan and M. Loncar, Opt. Express **19**, 18529 (2011).
17. HITRAN 2004 molecular spectroscopic database.
18. S. I. Shopova, R. Rajmangal, S. Holler, and S. Arnold, Appl. Phys. Lett. **98**, 243104 (2011).